JACS
JOURNAL OF THE AMERICAN CHEMICAL SOCIETY
Article
pubs.acs.org/JACS

The Pivotal Role of Oxyallyl Diradicals in Photo-Favorskii Rearrangements: Transient Spectroscopic and Computational Studies

Tomáš Šolomek,*[,†,‡] Dominik Heger,[†,‡] Bokolombe P. Ngoy,[†] Richard S. Givens,*[,§] and Petr Klán*[,†,‡]

[†]Department of Chemistry and [‡]Research Centre for Toxic Compounds in the Environment, Faculty of Science, Masaryk University, Kamenice 5, 625 00, Brno, Czech Republic

[§]Department of Chemistry, University of Kansas, 1251 Wescoe Hall Drive, 5010 Malott Hall, Lawrence, Kansas 66045, United States

Supporting Information

ABSTRACT: The photochemistry of the hydroxybenzocycloalkanonyl derivatives **6b–e** provides the triplet oxyallyl diradicals ^{3}**9** that decay via intersystem crossing to their more stable singlet isomers ^{1}**9**. Vibrationally resolved transient spectra of ^{3}**9** were recorded by pump–probe spectroscopy and laser flash photolysis. It was found that the ring strain dependent rate of intersystem crossing is the rate-limiting step in the formation of photo-Favorskii or solvolysis reaction products in water. The reactivities of open-shell singlet oxyallyls ^{1}**9a–e** determine the product ratios due to their relative abilities to form the corresponding cyclopropanones **10**. The smallest five-membered derivative, ^{1}**9b**, represents the first example of an oxyallyl diradicaloid that cannot form cyclopropanone **10b** or the isomeric allene oxide **13b**; instead, it is eventually trapped by water to form the sole solvolysis product **12b**. Our observations provide a comprehensive overview of the role of oxyallyl diradicals in reaction mechanisms and offer a new strategy to stabilize open-shell singlet diradicals.

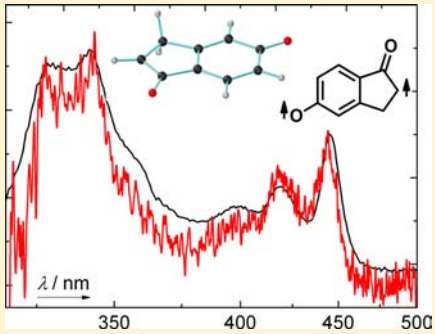

INTRODUCTION

Oxyallyls (**1**, in blue, Scheme 1) have been postulated as reactive intermediates in the formation and ring-opening reactions of cyclopropanones (**2**) and allene oxides (**3**).[1] They also have frequently been suggested as intermediates in some cycloaddition and rearrangement reactions, such as the Favorskii rearrangement,[2] the photo-Nazarov cyclization,[3] photorearrangement of cross-conjugated dienones,[4] and in prostaglandin biosynthesis.[5] Progress on the detection of oxyallyls has been slow and difficult until recently when the parent oxyallyl **1** was identified.[6] The $^1A_1$ ground state of **1** has diradicaloid character, and its lowest triplet state of $^3B_2$ symmetry is only 1.3 kcal mol^{-1} higher in energy. The vibrational band broadening observed for the $^1A_1$ state indicates that it is the transition state for a disrotatory ring closure to the more stable cyclopropanone **2**. Substituents on **1** affect the shape of its potential energy surface (PES). The oxyallyl diradicaloid becomes a shallow local minimum with an ultrashort lifetime (3.3 ps) as shown in photolysis of 2,4-bis-(spirocyclohexyl)cyclobutane-1,3-dione.[7] The lifetime was significantly extended when the dione was photolyzed as a crystalline solid, affording its absorption spectrum. Hess proposed that the more polar zwitterionic structure of **1** would be stabilized by tropylium ion conjugation in **4** (Scheme 1b), making it more stable than the valence-isomeric cyclopropanone **5**.[8]

Scheme 1. Primary Reactions of (a) the Singlet Oxyallyl Diradical 1 (in blue) and (b) the Stabilization of Oxyallyl Zwitterion in 4

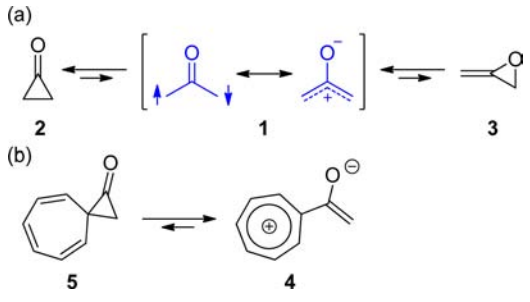

The photo-Favorskii rearrangement of the *p*-hydroxyphenacyl (pHP) derivative **6a** (Scheme 2) leads to *p*-hydroxyphenylacetic acid (**7a**) and a minor amount of *p*-hydroxybenzyl alcohol (**8a**) when a moderate to good leaving group (LG) is positioned adjacent to the phenacyl carbonyl.[9] The intermediacy of the triplet diradical ^{3}**9a** (in red, Scheme 2), an analogue of the oxyallyl diradical ^{3}**1** which subsequently decays via intersystem crossing, has been proposed.[10] Furthermore, formation of ^{3}**9a** has been recently proposed to be a major photorearrangement pathway for a chiral α-substituted *p*-hydroxybutanone (LG = a phenylacetate).[11] The subsequently formed cyclopropanone **10a** has been postulated

Received: July 26, 2013
Published: September 30, 2013

   dx.doi.org/10.1021/ja407588p | J. Am. Chem. Soc. 2013, 135, 15209–15215

Scheme 2. Photochemistry of 6[a]

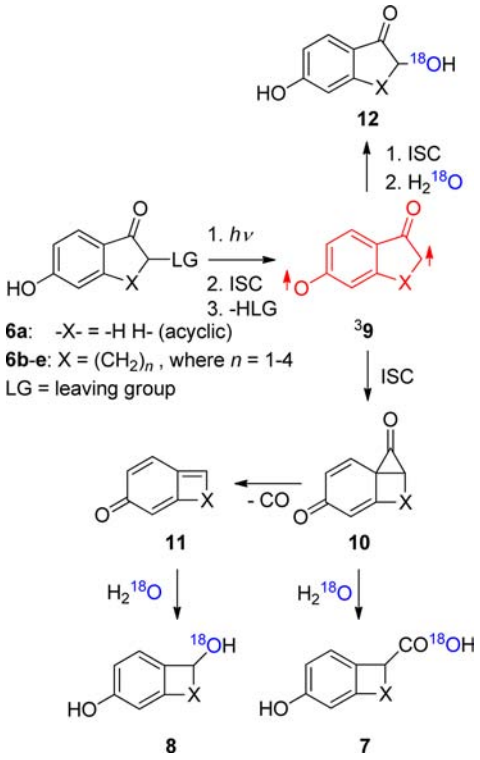

[a] The ^{18}O incorporation from $D_2{}^{18}O$ is indicated.[13]

several times.[9−13] However, unambiguous spectroscopic characterization of **10a** has not been reported to date. The formation of the *p*-quinone methide **11a**, observed in laser flash photolysis experiments, is thought to be initiated by decarbonylation of **10a**.[10a] The product ratio [**7a**]/[**8a**] increases with increasing water concentration in the solvent mixture suggesting that both are produced from the same cyclopropanone intermediate **10a**. Our recent study of the ring-strain effects on the rearrangement in a monotonic series of the hydroxybenzocycloalkanonyl derivatives **6b−e** to probe the intermediacy of **10** (Scheme 2) led to the discovery of a threshold for the Favorskii ring contraction at the cyclohexanone **6c** (n = 2) ring size.[13] The cyclopentanone **6b** (n = 1) requires the formation of a highly strained bicyclo[2.1.0]-pentanone **10b**. The inability to form **10b** essentially shuts down the reaction channel to **7** and **8**, and thereby the reaction is diverted toward the seldom observed solvolysis channel to form **12**. The origin of **12** and its possible relationship to triplet diradical ^{3}**9** (Scheme 2) remain to be established.

Here we report a detailed examination of the subtle, yet crucial roles played by both triplet and singlet oxyallyl diradicaloid intermediates, ^{3}**9** and ^{1}**9**, in the photochemical reactions of **6** and present the vibrationally resolved transient absorption spectra of the former. We provide spectroscopic evidence that the decay of ^{3}**9** is the rate-limiting step for both photo-Favorskii and solvolysis channels and demonstrate that the intermediacy of ^{1}**9** in the mechanism is necessary and sufficient for the product forming steps. Ring strain is shown to have a major influence on its stability which is a decisive factor in the partitioning of ^{1}**9** to products. We further propose that our analysis will be useful for developing new strategies for stabilized long-lived diradicaloids.

EXPERIMENTAL SECTION

Synthesis. The synthesis of the hydroxybenzocycloalkanonyl derivatives **6b** and **6c** (LG = OMs) was accomplished by a silver-promoted S_N2 displacement of the bromide by methanesulfonate in 2-bromo-5-hydroxyindanone and 2-bromo-6-hydroxytetralone, respectively, according to the previously reported procedure.[13]

Picosecond Pump−Supercontinuum Probe. Picosecond transient absorption spectra were measured with the pump−supercontinuum probe technique using a Ti:Sa laser system (775 nm, pulse energy 1.05 mJ, full width at half-maximum 150 fs, operating frequency 426 Hz). Part of the beam was fed into a NOPA. The output at 532 nm (upon compression) was frequency doubled by a β-barium borate (BBO) crystal to 266 nm and elicited pump pulses of 1 μJ energy and <150 fs pulse width. A probe beam continuum was generated by focusing the 775 nm beam in front of a CaF_2 plate with 4 mm path length that produced a supercontinuum probe beam spanning a wavelength range of 300−590 nm. The pump and probe beams were focused to a 0.2 mm spot on the sample that was flowing in an optical cell with a thickness of 0.4 mm. The probe beam as well as the reference beam, that passes through the solution in the absence of a pump beam, were spectrally dispersed and registered with two photodiode arrays (512 pixels). Transient absorption spectra were calculated from the ratio of the two beams. The pump−probe cross-correlation was <100 fs over the entire spectrum. To improve the signal-to-noise ratio, the data were averaged over multiple pump−probe scans (3−6 scans with 400 shots per temporal point). The time window of our apparatus for collecting the data spans ∼1.8 ns. The data were then analyzed by global analysis[14] and fitted with an appropriate kinetic model.

Nanosecond Laser Flash Photolysis. The LFP setup was operated in a right-angle arrangement of the pump and probe beams. Laser pulses of ≤700 ps duration at 266 nm (30−80 mJ) were obtained from an Nd:YAG laser and were dispersed over the 4 cm optical path of the quartz cell by a concave cylindrical lens.[15] The absorbance of the sample solutions was adjusted to 0.3−0.5 per cm at the wavelength of excitation. A pulsed 75 W xenon lamp was used as the source of white probe light. Kinetic detection at a single wavelength isolated by a monochromator in front of a photomultiplier and spectrographic detection (ICCD camera connected to a spectrometer equipped with 300 l/mm gratings blazed at 300 or 500 nm) of the transient absorptions was available. A fresh solution was used for each laser flash to avoid excitation of the photoproducts. Measurements were done at ambient temperature (20 ± 2 °C).

Quantum Chemical Calculations. For the purpose of modeling UV absorption spectra, the geometry optimization and the frequency calculations were carried out at the (U)B3LYP/6-31+G(d) level of theory. Electronic transitions were calculated using the time-dependent density functional theory (TD-DFT) approach employing the (U)B3LYP/6-31G(d,p) method. Complete UV−vis spectra were obtained using the linearized harmonic reflection principle as employed by Ončák et al.[16] The vibrationally resolved spectra were calculated at the TD-M06-2X/6-31G(d) level of theory using Franck−Condon analysis as implemented in Gaussian 09.[17] Solvent water was simulated as a polarizable continuum (PCM model). Nonequilibrium solvation was considered in calculations of electronic transitions that did not involve geometry optimizations in which equilibrium solvation was used.

We resorted to the composite CBS-QB3[18] and the G4[19] methods to get reliable comparison of the energies in the regions of the PES where open-shell singlet states do not preclude the use of single reference methods. All calculations described above were carried out with the Gaussian 09 electronic structure suite of programs.[20]

For processes that involve formation or decay of oxyallyl diradicaloid species, we used the multiconfigurational complete active space self-consistent field (CASSCF) method with the 6-31G* basis set to find stationary points. We checked that the geometries do not change significantly on enlarging the basis set. All geometry optimizations with CASSCF method as well as spin−orbit coupling calculations (see below) were carried out in a Molpro 2010 suite of

dx.doi.org/10.1021/ja407588p | J. Am. Chem. Soc. 2013, 135, 15209−15215

programs,[21] while the single-point energy calculations employing perturbation theory to account for the dynamic electron correlation were carried out with the CASPT2 method and the ANO-L-VTZP basis set with high-accuracy Cholesky decomposed two-electron integrals as implemented in Molcas 7.6.[22]

A combination of calculations with active spaces containing 10 electrons in 10 orbitals, CAS(10,10), and 12 electrons in 11 orbitals, CAS(12,11), was used to model a part of the PES describing diradicaloids or cyclopropanones and allene oxides, respectively. The (10,10) active space was composed of all π/π^* molecular orbitals (MOs) containing 10 π-electrons in the case of the diradicaloids. For cyclopropanones, one pair of π/π^*-MOs turns into a pair of σ- and σ^*-MOs of the newly formed C−C bond. For allene oxides, one of the π-MOs and the carbonyl oxygen nonbonding (p_y) orbital are involved in the formation of the new σ-C−O bond. The nonbonding orbital must, therefore, be included in the active space to describe the transition states that lead to formation of the C−O bond, and we enlarged the active space to (12,11). In order to compare energies, the active space used to construct the PES must be compatible for all species. Thus, we carried out calculations of allene oxides also with the (10,10) active space as a reference that did not contain a single π-MO (p_z) on carbonyl oxygen that has occupation number close to 1.99 in the (12,11) active space. The CASPT2 relative energies with CAS(12,11) reference wave function appeared to be within 1 kcal mol^{-1} when compared to those with the CAS(10,10) reference. The high-level composite G4 and the CBS-QB3 methods then served to ensure that the small incompatibilities of active spaces did not affect the chemical conclusions based on multireference calculations (see Supporting Information). A similar approach has recently been successfully employed.[23] It was found that the CASPT2 relative energies of closed-shell species are lower and within 2 kcal mol^{-1} when compared to the G4 and CBS-QB3 energies. All the MOs in the active spaces used are depicted in Figures S13−S16.

We used CASSCF state-averaged orbitals in calculations of the S/T intersections and spin−orbit coupling constants. These were calculated with a CAS(10,10)/6-31G(d) wave function using the Breit−Pauli Hamiltonian with one-center approximation used for one- and two-electron spin−orbit integrals as implemented in the Molpro 2010 suite of programs.[21] The more accurate full two-electron treatment was checked in one case and proved to yield nearly identical results.

RESULTS

The transient UV−vis spectra were measured by laser irradiation of aqueous acetate buffer solutions of **6b,c** of various compositions (20 mM acetate buffer, pH = 4.9 and 3 M acetate buffer, pH = 3.6; pH was measured using the glass electrode). A small addition of acetonitrile was necessary to increase the solubility of **6** (H_2O/CH_3CN (95: 5, v/v) for nanosecond LFP and H_2O/CH_3CN (66: 33, v/v) for picosecond pump−probe measurements). The lifetimes and the rate constants are given in the following format: mean ± standard deviation of the mean with number of measurements (m) enclosed in parentheses.

Pump−Probe Spectroscopy. The data from pump−probe measurements were analyzed starting at 6 ps after the pump pulse to avoid any spectral interference from intersystem crossing (ISC) of singlet excited states of **6b,c**. The lifetime of the singlet excited state of a related system, *p*-hydroxyacetophenone (pHA), was reported to be 3.4 ± 0.4 ps.[24] The initial spectrum obtained by global analysis of measured data possesses a broad band with maximum at 425−430 nm for both **6b,c** (Figures 1, S1 and S2) and was assigned to the triplet state of **6b,c** by analogy with our previous studies of pHP diethyl phosphate[10a] and pHA.[24] The decay of the triplet excited state of **6** was characterized by first-order decay rate constants k: $k_{6b} = (1.5 \pm 0.2) \times 10^{11}$ s^{-1} (m = 2; 20 mM acetate buffer, pH = 4.9) and $k_{6c} = (8.8 \pm 0.8) \times 10^{9}$ s^{-1} (3 M acetate buffer, pH = 3.6) for **6b** and **6c**, respectively. Spectra with weak absorption bands that contained several distinct maxima λ_{max} = 445, 419, 398, 359, 342, 328 nm and 453, 424, 348, 335 nm were obtained for **6b** and **6c**, respectively. The spectra, shown in Figure 1, compare favorably with those obtained previously by excitation of **6a** and assigned to ^{3}**9a**.[10a] The TD-DFT calculations of the absorption spectra of ^{3}**9b,c** (Figure S3) support the presumption that the triplet diradicals are formed. Calculations show that there are two intense electronic transitions separated by ∼7000 cm^{-1} (Table S1). Franck−Condon analysis of the first series of absorption bands (450−400 nm) revealed the pronounced involvement of two vibrational modes besides the 0−0 transition (see Figure S4). Thus, we attribute the separation of the absorption bands in ^{3}**9b** (∼1300 cm^{-1}) and ^{3}**9c** (∼1500 cm^{-1}) to vibrational progressions. The decay of the triplet state of **6b** in a 3 M acetate buffer (pH = 3.6) was accompanied by a more complex kinetic behavior leading finally to the identical transient absorption spectrum (Figure S5) as observed in a 20 mM acetate buffer (pH = 4.9).

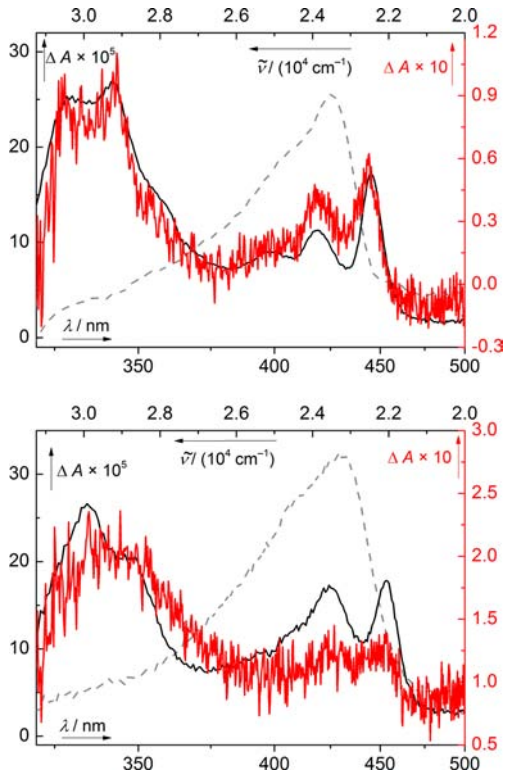

Figure 1. Transient spectra of the triplet diradicals ^{3}**9b** (top) and ^{3}**9c** (bottom) obtained by the global analysis of pump−probe data (in black; H_2O/CH_3CN (66:33, v/v), 3 M acetate buffer, pH = 3.6) and from nanosecond LFP (in red; H_2O/CH_3CN (99:1, v/v), 3 M acetate buffer, pH = 3.6; 1 ns after the laser pulse with 3 ns accumulation time). The dashed gray spectra (their intensity was reduced by a factor of 2.5; see Figures S1 and S2 for the original data) correspond to the triplet states of **6b** (top) and **6c** (bottom).

The decay of both ^{3}**9b** and ^{3}**9c** occurs on a nanosecond time scale (see below) that precludes a proper fit of the kinetic data for the former species due to its lifetime which is longer than the experimental limit of our pump−probe apparatus (∼1.8 ns). The lifetime of the latter and the transient absorption spectrum of the subsequently formed species were estimated as follows. We assumed that any product of decay of ^{3}**9c** does not absorb in the 400−500 nm spectral window. Under these

dx.doi.org/10.1021/ja407588p | J. Am. Chem. Soc. 2013, 135, 15209−15215

conditions, the transient absorption data in this transparent region were fitted with two exponential functions. The resulting rate constant $k_{9c} = 3.5 \times 10^8$ s^{-1} for decay of ^{3}**9c** was used to fit the data in the full spectral window resulting in three distinct transient spectra shown in Figure S2. The final spectrum (highlighted in green) matched the spectrum measured independently (pH = 12) for the conjugate base of **12c** (Scheme 3, Figure S6).

Scheme 3. Formation and Hypothetical Decay Channels Available to ^{1}9

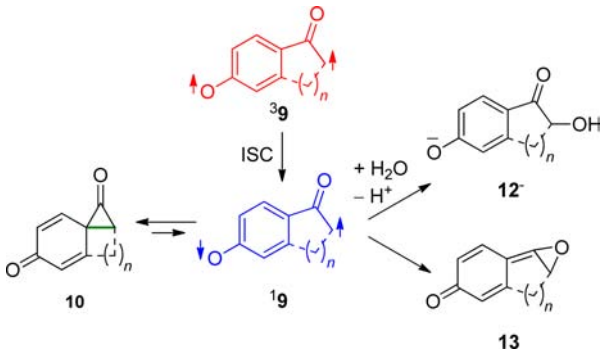

Nanosecond Laser Flash Photolysis. A spectrum obtained by excitation of **6b** (3 M acetate buffer, pH = 3.6) 1 ns after the laser pulse with 3 ns accumulation time corresponds to the spectrum of ^{3}**9b** from the pump–probe experiment. The first-order rate constant for decay of ^{3}**9b**, $k_{9b} = (7.2 \pm 0.3) \times 10^7$ s^{-1} (m = 17), was measured at 443, 419, and 343 nm and found to be independent of the buffer concentration (Figure S7). A weak but still distinguishable transient signal of ^{3}**9c** was observed by excitation of **6c** under the same experimental conditions. Both spectra are compared to those obtained by pump–probe experiments in Figure 1. The first-order rate constant for decay of ^{3}**9c**, $k_{9c} = (2.6 \pm 1.2) \times 10^8$ s^{-1} (m = 3), was measured at 450 nm. An average rate constant k_{9c}(average) = $(3 \pm 2) \times 10^8$ s^{-1} was estimated from the data both from the pump–probe and the LFP experiments.

Upon excitation of **6b**, another transient with an absorption maximum at 335 nm was formed with the rate constant that is identical to that of the decay of ^{3}**9b** (Figure S8). The spectrum measured 30 ns after the laser flash of a fresh solution of **6b** (20 mM acetate buffer, pH = 4.9) compared well with that of **12b**$^-$ measured in basic aqueous solution of **12b** (pH = 9.6). The same spectrum was also obtained from pump–probe data (in 6–1800 ps temporal range) that must be analyzed, however, by fitting with two rate constants with one constrained to the value of the rate constant of decay of ^{3}**9b** measured accurately in the LFP experiment ($k_{9b} = 7.0 \times 10^7$ s^{-1}). The fitting procedure converged well, resulting in the rate constant $k_{6b} = (1.3 \pm 0.1) \times 10^{11}$ s^{-1} for the decay of triplet **6b**, which is identical within the experimental error to that obtained by the direct, unconstrained analysis of our pump–probe experimental data (see above). The three transient spectra that resulted from this analysis are those of the triplet of **6b**, ^{3}**9b**, and **12b**$^-$. The spectra of **12b**$^-$ obtained from the experiments described above are shown in Figure S8. A similar analysis was performed for the decay of ^{3}**9c** (Figure S2). We found that **12b**$^-$ and **12c**$^-$ are protonated by the buffer (20.0, 2.0, and 0.5 mM acetate buffer, pH = 4.7 ± 0.2) at nearly diffusion-controlled rates with bimolecular rate constants for protonation k_{12b}(AcOH) = $(3.4 \pm 0.5) \times 10^9$ M^{-1} s^{-1} (m = 9) and k_{12c}(AcOH) = $(4.3 \pm 0.4) \times 10^9$ M^{-1} s^{-1} (m = 8), respectively (see Table S2 and Figure S9).

Quantum Chemical Calculations. The CASSCF calculations showed that diradicals ^{3}**9c–e** are nonplanar species with the plane of the carbonyl group twisted (by 11–47°) with respect to the plane of the oxyphenyl ring (the C_{Ar}–CO dihedral angle). Diradicals ^{3}**9a,b** possess planar energy minima. However, the carbonyl group of **9a** is significantly twisted at the T_1/S_0 surface intersection (by 32.5°, Figure 2) that is 3.2 kcal mol^{-1} above the energy minimum of ^{3}**9a**. The spin–orbit coupling constants in ^{3}**9a** are nearly zero at the planar geometry and increase to a maximum value when the C_{Ar}–CO dihedral angle reaches ~35° (Figure 3). The maximum value of the spin–orbit coupling at the T_1/S_0 intersection point in **9a** is 0.438 cm^{-1}.

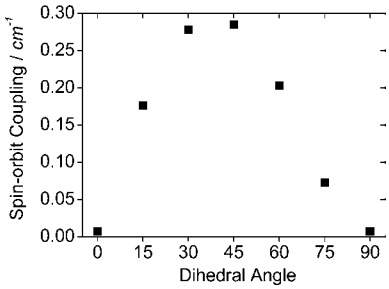

Figure 3. The dependence of the singlet–triplet spin–orbit coupling on the C_{Ar}–CO bond twist in ^{3}**9a**; the dihedral angle is for the rotation of the carbonyl plane with respect to the oxyphenyl ring plane.

The energy minima geometries of the singlet diradicaloids ^{1}**9** are similar to those of the triplet congeners ^{3}**9**. The Mulliken charges of ^{1}**9a** and ^{3}**9a** are essentially identical (Figure S11). The occupation numbers of HOMO and HOMO+1 orbitals of ^{1}**9a** and the parent oxyallyl **1** are depicted in Figure 4 and are compared to the remaining members of ^{1}**9** series in Table S3. The adiabatic singlet–triplet energy gaps calculated for the complete series of diradicals ^{1}**9** are summarized in Table 1.

The transition states TS[^{1}**9** → **10**] connecting the singlet diradicaloids with the "Favorskii" bicyclo[*n*.1.0]propanones **10** (Scheme 3) lie within a few kcal mol^{-1} near the energy minima of ^{1}**9** (Table 1). However, we were unable to optimize an energy minimum for **10b**. All our attempts resulted in the

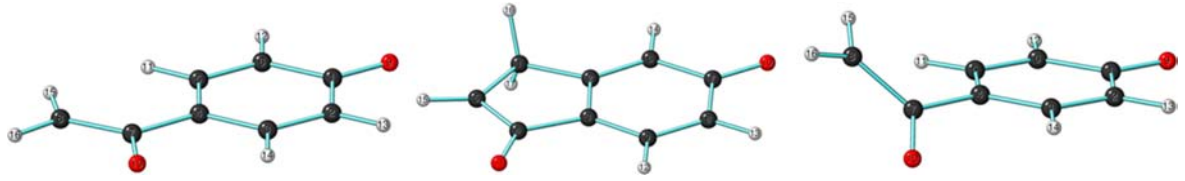

Figure 2. The structures of the planar triplet diradicals: ^{3}**9a** (left), ^{3}**9b** (middle), and the T_1/S_0 surface crossing point in **9a** (right).

dx.doi.org/10.1021/ja407588p | J. Am. Chem. Soc. 2013, 135, 15209–15215

Table 1. Summary of the Calculated Energies[a] Related to Scheme 3 and Lifetimes of ^{3}9 from the Time-Resolved Experiments

ring size	E_{S-T}[b]	τ, ns	ΔH^b (10)	ΔH^b (TS[^{1}9→10])	ΔH^b (13)	ΔH^b (TS[^{1}9→13])
no ring (**9a**)	−0.04	0.56 ± 0.12	−8.3	2.4	−6.6	14.5
5 (**9b**)	4.9	13.9 ± 0.6	–[c]	–[c]	45.5	45.5[d]
6 (**9c**)	1.2	3 ± 2	−2.8	1.7	17.1	20.9
7 (**9d**)	0.4	–[f]	−10.8	0.05	3.3[e]	–[f]
8 (**9e**)	−0.6	–[f]	−10.8	−0.3	−9.0[e]	–[f]

[a]Energies at 0 K in kcal mol^{-1} with respect to the energy of the corresponding singlet oxyallyl diradicaloid ^{1}**9**. [b]Calculated at the CASPT2/ANO-L-VTZP level of theory using the CAS(10,10) or CAS(12,11) reference wave functions on the CASSCF/6-31G(d) geometries. See the Experimental section for further details. The ZPVE correction is included with no scaling. [c]Does not represent a stationary point on the PES at the level of theory employed here. [d]Calculated energy difference between **13b** and the transition state TS[^{1}**9b** → **13b**] is <0.01 kcal mol^{-1}. [e]Based on G4 calculations. [f]Not available.

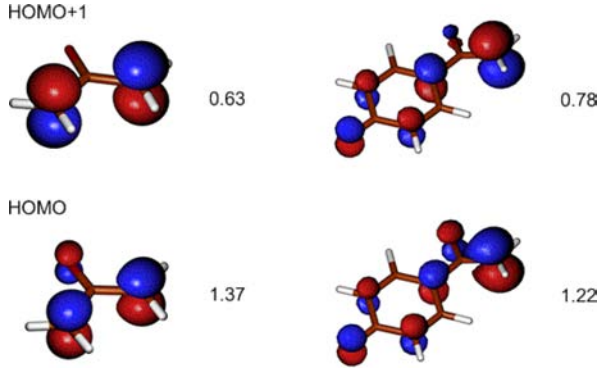

Figure 4. HOMO and HOMO+1 molecular orbitals of ^{1}**1** (left) and ^{1}**9a** (right) from CAS(10,10)/6-31G(d) calculations. The orbital occupation numbers are shown next to the corresponding orbitals.

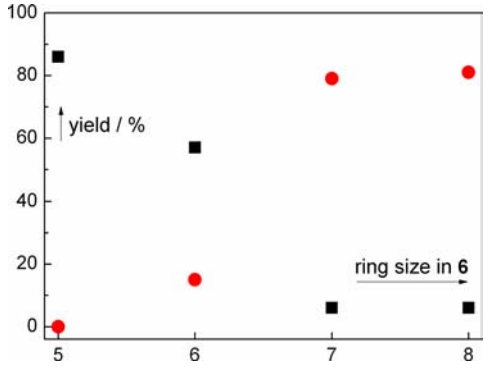

Figure 5. The dependence of photoproduct chemical yields (black: **12**; red: the sum of the yields of **7** and **8**) on the ring size of **6** irradiated in water/acetonitrile (70:30, v/v). Adopted from ref 13.

spontaneous C−C bond cleavage in **10b** (highlighted in green in Scheme 3) to form ^{1}**9b**.[13] The relaxed CASPT2 PES scan along this C−C bond length coordinate on CAS(10,10)/6-31G(d) geometries is shown in Figure S12.

The transition states TS[^{1}**9** → **13**] that lead to the formation of allene oxides **13** (Scheme 3) are energetically higher compared to the transition states TS[^{1}**9** → **10**] that connect ^{1}**9** with cyclopropanones **10** (Table 1). We found that the energy of the TS[^{1}**9b** → **13b**] transition state is very high and essentially identical (within 0.01 kcal mol^{-1}) to the energy of **13b**. The energies of larger derivatives **13d,e** were estimated by comparison to the energies of closed-shell cyclopropanones **10** using the high-level G4 composite method.

DISCUSSION

It is well established that the photolysis of **6a** leads to leaving group departure from the triplet state[9e,25] with a concomitant formation of triplet oxyallyl diradical ^{3}**9a** (Scheme 2).[10] The lifetime of ^{3}**9a** (~600 ps) corresponds to the rate of formation of the final rearranged product, *p*-hydroxyphenylacetic acid **7a**.[25d] We, however, have already reported that the rearrangement cannot occur on the triplet energy surface due to the considerable barrier to ring closure to ^{3}**10a**, leaving ^{3}**9a** to decay by ISC.[10a,13] The relationship of ^{3}**9a** and the products therefore requires the existence of one or more additional intermediates.

Ring strain has proven to have a profound impact on the rearrangements of **6b−e**. As the ring size in **6b−e** decreased, the composition of the product mixture (Figure 5) strongly diverged from that obtained for the photolysis of **6a** which is completely free of ring strain.[13] The nature of the leaving group did not affect the product distribution; only the disappearance quantum yields changed. Therefore, both the photo-Favorskii and solvolytic reaction channels are originating from an intermediate that is formed after the leaving group is released.

This is corroborated by current pump−probe and nanosecond LFP experiments with **6b,c** that provide unequivocal evidence that ^{3}**9b,c** are formed upon irradiation as reported in our earlier studies of **6a**. The lifetimes of ^{3}**9b,c** are significantly longer than that measured for ^{3}**9a** and increase with decreasing ring sizes of **6b,c**. The presence of the ring constrains the ability of ^{3}**9b,c** to energetically approach the T_1/S_0 intersection where appreciable spin−orbit coupling facilitates the intersystem crossing (Figures 2 and 3). The planarity restriction imposed by the five-membered ring and the largest singlet−triplet energy splitting in **9b** represent a limiting case, and as a consequence, the lifetime of ^{3}**9b** is prolonged by a factor of ~25.

The diradical ^{3}**9b** strikingly leads to the formation of **12b**, completely avoiding the photo-Favorskii reaction channel. Clearly, both reaction channels then share another common intermediate that is formed after ISC of ^{3}**9**, and whose decay is strongly influenced by ring strain. It must precede the step in which the reaction partitions to the formation of **7** and **8** because their ratio depends only on water concentration, i.e., the decay of **10**.[10a] We identified ring strain as a critical factor for formation of **10b** that, therefore, essentially blocks off the photo-Favorskii channel. Cyclopropanones **10c−e** must be formed from the triplet oxyallyl diradicals ^{3}**9** via this common intermediate from which the PES bifurcates toward either the solvolytic or the photo-Favorskii reaction channels. We now suggest that this common intermediate is, in fact, an open-shell singlet oxyallyl diradicaloid ^{1}**9**. Interestingly, the singlet and triplet oxyallyl species were originally postulated by Phillips and

dx.doi.org/10.1021/ja407588p | J. Am. Chem. Soc. 2013, 135, 15209−15215

co-workers.[26] The authors did suggest that another intermediate "B" was required based on their kinetic modeling of the decay rates. However, they did not further investigate or identify it.[26b] Our results clearly demonstrate that diradicaloid ^{1}**9** is that intermediate.

The occupation numbers of frontier MOs suggest a pronounced diradicaloid character in the ^{1}**9** series when compared to the parent oxyallyl **1** (Figure 4, Table S3) due to the stabilization offered by the unsaturated ring. The diradicaloid character increases with increasing ring size that compels the carbonyl and oxyphenyl groups to adopt increasingly larger dihedral angles. A pure diradical would result when the π-MOs of both the carbonyl and oxyphenyl groups were disjoint in a perpendicular spatial arrangement.

Small energy barriers that connect ^{1}**9** with the corresponding cyclopropanones **10** (except ^{1}**9b**; Scheme 3, Table 1) suggest an ultrafast ring closure in accord with the observation of Kuzmanich and co-workers.[7] Therefore, the barrier imposed by ISC of ^{3}**9** also kinetically limits formation of the final photo-Favorskii product **7** (note that the rate-limiting step for formation of **8** is hydration of **11**). Our calculations are in excellent agreement with the experimental observation that ^{1}**9b** faces an insurmountable barrier to form a highly strained Favorskii intermediate **10b**. Consequently, the photo-Favorskii channel is closed at the stage of the singlet oxyallyl diradicaloid, which must subsequently yield **12b**. Moderate ring strain lowers the energy of ^{1}**9c** close enough to **10c** such that their rapid equilibration might be responsible for the intermediate distribution of products observed for **6c** (Figure 5).

Shepp and co-workers suggested that allene oxides could be intermediates in the solvolysis of singlet oxyallyls.[27] The formation of allene oxides **13**, however, is strongly endothermic for the small ring derivatives and requires surmounting a high-energy barrier that is incompatible with the ultrafast formation of final products. In such a case, allene oxides are avoided, and instead the intermediate ^{1}**9** follows a pathway of direct nucleophilic attack of water, the only available reaction under the conditions we have explored. This is supported by time-resolved measurements that clearly show that fast ISC of ^{3}**9b,c** is the rate-limiting step in formation of **12b,c**$^-$ which are subsequently protonated by a general acid to yield **12b,c**.

In addition, our calculations, for the series of cycloalkanones studied here, suggest that both **10b** and **13b** are only hypothetical species. Therefore, to the best of our knowledge, ^{1}**9b** is the first example of a singlet oxyallyl diradicaloid that is incapable of forming either the corresponding cyclopropanone or the isomeric allene oxide. It is anticipated that singlet diradicaloids with restrictive features similar to those of **9b** will be long-lived in the absence of nucleophiles. We are currently investigating the rational design of stable oxyallyl and other diradicaloids based on the principles of ring strain[28] and aromatic stabilization introduced in this work.

CONCLUSIONS

Scheme 4 portrays a combined illustration of the available channels consistent with this and all previous investigations of the rearrangement of the pHP chromophore when it is imbedded in the structural constraints of a ring. The leaving group liberation from triplet **6** generates the triplet oxyallyl diradical ^{3}**9** that is planar and achiral, thus responsible for the racemization of a chiral α-substituted ketone group. The diradical ^{3}**9** undergoes relatively rapid, though rate-limiting intersystem crossing to the singlet oxyallyl diradicaloid ^{1}**9** that closes very rapidly to the elusive cyclopropanone **10**. Cyclopropanone **10** is then trapped by water to yield the rearranged acid **7** or decarbonylates to give **11** followed by a relatively slow hydration to give **8**. When ring strain interferes with the disrotatory ring closure of ^{1}**9**, competition of a direct nucleophilic attack of water and subsequent proton shuffling lead to the product **12**.

Scheme 4. Mechanism of the Photo-Favorskii Reaction Highlighting the Rearrangement Events

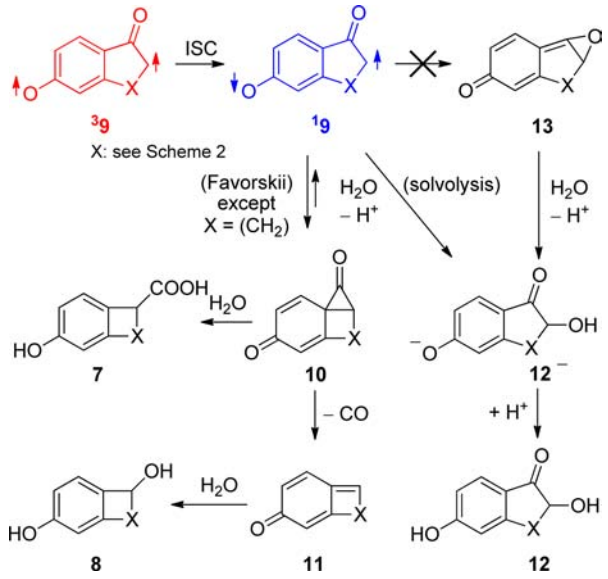

ASSOCIATED CONTENT

Supporting Information

Experimental and computational spectra of the intermediates; kinetic flash photolysis data; quantum chemical calculations. This material is available free of charge via the Internet at http://pubs.acs.org.

AUTHOR INFORMATION

Corresponding Authors

tom.solomek@gmail.com
givensr@ku.edu
klan@sci.muni.cz

Notes

The authors declare no competing financial interest.

ACKNOWLEDGMENTS

Support for this work was provided by the Grant Agency of the Czech Republic (13-25775S), the project CETOCOEN (CZ.1.05/2.1.00/01.0001) granted by the European Regional Development Fund (P.K.), and R01 GM72910 (R.S.G.). We also acknowledge University of Fribourg for the computational resources (T.S.). We thank Pavel Friš for his help with the laser flash photolysis experiments.

REFERENCES

(1) (a) Crandall, J. K.; Machleder, W. H. *J. Am. Chem. Soc.* **1968**, *90*, 7347. (b) Cordes, M. H. J.; Berson, J. A. *J. Am. Chem. Soc.* **1992**, *114*, 11010. (c) Hrovat, D. A.; Rauk, A.; Sorensen, T. S.; Powell, H. K.; Borden, W. T. *J. Am. Chem. Soc.* **1996**, *118*, 4159. (d) Hess, B. A.; Eckart, U.; Fabian, J. *J. Am. Chem. Soc.* **1998**, *120*, 12310.

(2) (a) Aston, J. G.; Newkirk, J. D. *J. Am. Chem. Soc.* **1951**, *73*, 3900. (b) Hamblin, G. D.; Jimenez, R. P.; Sorensen, T. S. *J. Org. Chem.* **2007**, *72*, 8033.
(3) Leitich, J.; Heise, I.; Werner, S.; Kruger, C.; Schaffner, K. *J. Photochem. Photobiol., A* **1991**, *57*, 127.
(4) (a) Zimmerman, H. E.; Schuster, D. I. *J. Am. Chem. Soc.* **1962**, *84*, 4527. (b) Crandall, J. K.; Haseltine, R. P. *J. Am. Chem. Soc.* **1968**, *90*, 6251. (c) Matlin, A. R.; Lahti, P. M.; Appella, D.; Straumanis, A.; Lin, S.; Patel, H.; Jin, K.; Schrieber, K. P.; Pauls, J.; Raulerson, P. *J. Am. Chem. Soc.* **1999**, *121*, 2164.
(5) Hess, B. A.; Smentek, L.; Brash, A. R.; Cha, J. K. *J. Am. Chem. Soc.* **1999**, *121*, 5603.
(6) (a) Ichino, T.; Villano, S. M.; Gianola, A. J.; Goebbert, D. J.; Velarde, L.; Sanov, A.; Blanksby, S. J.; Zhou, X.; Hrovat, D. A.; Borden, W. T.; Lineberger, W. C. *Angew. Chem., Int. Ed.* **2009**, *48*, 8509. (b) Ichino, T.; Villano, S. M.; Gianola, A. J.; Goebbert, D. J.; Velarde, L.; Sanov, A.; Blanksby, S. J.; Zhou, X.; Hrovat, D. A.; Borden, W. T.; Lineberger, W. C. *J. Phys. Chem. A* **2011**, *115*, 1634.
(7) Kuzmanich, G.; Spänig, F.; Tsai, C.-K.; Um, J. M.; Hoekstra, R. M.; Houk, K. N.; Guldi, D. M.; Garcia-Garibay, M. A. *J. Am. Chem. Soc.* **2011**, *133*, 2342.
(8) Hess, B. A. *J. Am. Chem. Soc.* **2002**, *124*, 920.
(9) (a) Anderson, J. C.; Reese, C. B. *Tetrahedron Lett.* **1962**, 1. (b) Givens, R. S.; Park, C. H. *Tetrahedron Lett.* **1996**, *37*, 6259. (c) Park, C. H.; Givens, R. S. *J. Am. Chem. Soc.* **1997**, *119*, 2453. (d) Klán, P.; Šolomek, T.; Bochet, C. G.; Blanc, A.; Givens, R.; Rubina, M.; Popik, V.; Kostikov, A.; Wirz, J. *Chem. Rev.* **2012**, *113*, 119. (e) Givens, R. S.; Conrad, P. G.; Hellrung, B.; Rajesh, C. S.; Ramseier, M.; Wirz, J. *J. Am. Chem. Soc.* **2000**, *122*, 9346. (f) Givens, R. S.; Rubina, M.; Wirz, J. *Photochem. Photobiol. Sci.* **2012**, *11*, 472.
(10) (a) Givens, R. S.; Heger, D.; Hellrung, B.; Kamdzhilov, Y.; Mac, M.; Conrad, P. G.; Cope, E.; Lee, J. I.; Mata-Segreda, J. F.; Schowen, R. L.; Wirz, J. *J. Am. Chem. Soc.* **2008**, *130*, 3307. (b) Stensrud, K.; Noh, J.; Kandler, K.; Wirz, J.; Heger, D.; Givens, R. S. *J. Org. Chem.* **2009**, *74*, 5219.
(11) Givens, R. S.; Rubina, M.; Stensrud, K. F. *J. Org. Chem.* **2012**, *78*, 1709.
(12) Zhang, K.; Corrie, J. E. T.; Munasinghe, V. R. N.; Wan, P. *J. Am. Chem. Soc.* **1999**, *121*, 5625.
(13) Kammath, V. B.; Šolomek, T.; Ngoy, B. P.; Heger, D.; Klán, P.; Rubina, M.; Givens, R. S. *J. Org. Chem.* **2012**, *78*, 1718.
(14) Klán, P.; Wirz, J. *Photochemistry of organic compounds: From concepts to practice*; 1st ed.; John Wiley & Sons Ltd.: Chichester, 2009.
(15) Bonneau, R.; Wirz, J.; Zuberbuhler, A. D. *Pure Appl. Chem.* **1997**, *69*, 979.
(16) Ončák, M.; Šištík, L.; Slavíček, P. *J. Chem. Phys.* 2010, *133*.
(17) Barone, V.; Bloino, J.; Biczysko, M.; Santoro, F. *J. Chem. Theory Comput.* **2009**, *5*, 540.
(18) Montgomery, J. A.; Frisch, M. J.; Ochterski, J. W.; Petersson, G. A. *J. Chem. Phys.* **1999**, *110*, 2822.
(19) Curtiss, L. A.; Redfern, P. C.; Raghavachari, K. *J. Chem. Phys.* **2007**, *126*, 084108.
(20) Frisch, M. J.; Trucks, G. W.; Schlegel, H. B.; Scuseria, G. E.; Robb, M. A.; Cheeseman, J. R.; Scalmani, G.; Barone, V.; Mennucci, B.; Petersson, G. A.; Nakatsuji, H.; Caricato, M.; Li, X.; Hratchian, H. P.; Izmaylov, A. F.; Bloino, J.; Zheng, G.; Sonnenberg, J. L.; Hada, M.; Ehara, M.; Toyota, K.; Fukuda, R.; Hasegawa, J.; Ishida, M.; Nakajima, T.; Honda, Y.; Kitao, O.; Nakai, H.; Vreven, T.; Montgomery, J. A., Jr. ; Peralta, J. E.; Ogliaro, F.; Bearpark, M.; Heyd, J. J.; Brothers, E.; ; Kudin, K. N.; Staroverov, V. N.; Kobayashi, R.; Normand, J.; Raghavachari, K.; Rendell, A.; Burant, J. C.; Iyengar, S. S.; Tomasi, J.; Cossi, M.; Rega, N.; Millam, J. M.; Klene, M.; Knox, J. E.; Cross, J. B.; Bakken, V.; Adamo, C.; Jaramillo, J.; Gomperts, R.; Stratmann, R. E.; Yazyev, O.; Austin, A. J.; Cammi, R.; Pomelli, C.; Ochterski, J. W.; Martin, R. L.; Morokuma, K.; Zakrzewski, V. G.; Voth, G. A.; Salvador, P.; Dannenberg, J. J.; Dapprich, S.; Daniels, A. D.; Farkas, Ö.; Foresman, J. B.; Ortiz, J. V.; Cioslowski, J.; Fox, D. J. *Gaussian 09*, rev. C.2; Gaussian, Inc.: Wallingford, CT, 2009.
(21) Werner, H.-J.; Knowles, P. J.; Knizia, G.; Manby, F. R.; Schütz, M.; Celani, P.; Korona, T.; Lindh, R.; Mitrushenkov, A.; Rauhut, G.; Shamasundar, K. R.; Adler, T. B.; Amos, R. D.; Bernhardsson, A.; Berning, A.; Cooper, D. L.; Deegan, M. J. O.; Dobbyn, A. J.; Eckert, F.; Goll, E.; Hampel, C.; Hesselmann, A.; Hetzer, G.; Hrenar, T.; Jansen, G.; Köppl, C.; Liu, Y.; Lloyd, A. W.; Mata, R. A.; May, A. J.; McNicholas, S. J.; Meyer, W.; Mura, M. E.; Nicklaß, A.; O'Neill, D. P.; Palmieri, P.; Pflüger, K.; Pitzer, R.; Reiher, M.; Shiozaki, T.; Stoll, H.; Stone, A. J.; Tarroni, R.; Thorsteinsson, T.; Wang, M.; Wolf, A. *MOLPRO*, ver. 2010.1; University College Cardiff Consultants Limited: Cardiff, U.K., 2010.
(22) Aquilante, F.; De Vico, L.; Ferré, N.; Ghigo, G.; Malmqvist, P.-Å.; Neogrády, P.; Pedersen, T. B.; Pitonak, M.; Reiher, M.; Roos, B. O.; Serrano-Andrés, L.; Urban, M.; Veryazov, V.; Lindh, R. *J. Comput. Chem.* **2010**, *31*, 224.
(23) Nunes, C. M.; Reva, I.; Melo, T.; Fausto, R.; Šolomek, T.; Bally, T. *J. Am. Chem. Soc.* **2011**, *133*, 18911.
(24) Klíčová, L.; Šebej, P.; Šolomek, T.; Hellrung, B.; Slavíček, P.; Klán, P.; Heger, D.; Wirz, J. *J. Phys. Chem. A* **2012**, *116*, 2935.
(25) (a) Ma, C. S.; Chan, W. S.; Kwok, W. M.; Zuo, P.; Phillips, D. L. *J. Chem. Phys. B* **2004**, *108*, 9264. (b) Ma, C. S.; Zuo, P.; Kwok, W. M.; Chan, W. S.; Kan, J. T. W.; Toy, P. H.; Phillips, D. L. *J. Org. Chem.* **2004**, *69*, 6641. (c) Ma, C. S.; Kwok, W. M.; Chan, W. S.; Zuo, P.; Kan, J. T. W.; Toy, P. H.; Phillips, D. L. *J. Am. Chem. Soc.* **2005**, *127*, 1463. (d) Ma, C. S.; Kwok, W. M.; Chan, W. S.; Du, Y.; Kan, J. T. W.; Toy, P. H.; Phillips, D. L. *J. Am. Chem. Soc.* **2006**, *128*, 2558.
(26) (a) Chen, X. B.; Ma, C. S.; Kwok, W. M.; Guan, X. G.; Du, Y.; Phillips, D. L. *J. Phys. Chem. B* **2007**, *111*, 11832. (b) Cao, Q.; Guan, X.; George, M. W.; Phillips, D. L.; Ma, C.; Kwok, W. M.; Li, M.; Du, Y.; Sun, X.-Z.; Xue, J. *Faraday Discuss.* **2010**, *145*, 171.
(27) Clay, M. D.; Durber, J.; Schepp, N. P. *Org. Lett.* **2001**, *3*, 3883.
(28) (a) Kuzmanich, G.; Garcia-Garibay, M. A. *J. Phys. Org. Chem.* **2011**, *24*, 883. (b) Abe, M.; Furunaga, H.; Ma, D.; Gagliardi, L.; Bodwell, G. J. *J. Org. Chem.* **2012**, *77*, 7612.